Chemistry Europe
European Chemical Societies Publishing

WILEY VCH

Excellence in Chemistry Research

Announcing our new flagship journal

- Gold Open Access
- Publishing charges waived
- Preprints welcome
- Edited by active scientists

Meet the Editors of *ChemistryEurope*

Luisa De Cola
Università degli Studi di Milano Statale, Italy

Ive Hermans
University of Wisconsin-Madison, USA

Ken Tanaka
Tokyo Institute of Technology, Japan

ChemPlusChem

Research Article
doi.org/10.1002/cplu.202200457

Chemistry Europe
European Chemical Societies Publishing

www.chempluschem.org

Special Collection

Unraveling the Role of Nickel Nanoparticles Functionalization in the Electronic Properties and Structural Features of 2D Black Phosphorene Exposed to Ambient Conditions

Matteo Vanni,[a] Manuel Serrano-Ruiz,[a] Jonathan Filippi,[a] Maria Cristina Salvatici,[a] Emiliano Fonda,[b] Maurizio Peruzzini,[a] and Maria Caporali*[a]

Layered black phosphorus (BP) is endowed with peculiar chemico-physical properties that make it a highly promising candidate in the field of electronics. Nevertheless, as other 2D materials with atomic scale thickness, it suffers from easy degradation under ambient conditions. Herein, it is shown that the functionalization of BP with preformed and *in situ* grown Ni NPs, affects the electronic properties of the material. In particular, Ni functionalization performed *in situ* leads to a narrowing of the average BP band gap from 1.15 to 0.95 eV and to a marked shift in the conduction band maximum from −0.33 V to −0.07 V, which, in turn, improve the ambient stability. Structural studies carried out by XAS can well distinguish the two nanohybrids and reveal that once Ni NPs are grown on BP nanosheets, a Ni-P coordinative bond is formed, featuring a short Ni-P distance of 2.27 Å, which is not observed when preformed Ni NPs are immobilized on BP. Comparing the XANES and EXAFS spectra of fresh and aged samples of both nanohybrids, suggests that the interaction between Ni and P atoms results in a stabilization effect exerted via a dual electronic and redox mechanism, that infers a much superior ambient stability to BP, even if the surface functionalization is far to achieve a full coverage.

Introduction

Since its discovery in 2014 exfoliated black phosphorus, named hereafter BP, has gained an increasing interest among bidimensional materials and semiconductors thanks to its exceptional physicochemical properties.[1] The surface decoration of BP with metal nanoparticles[2] has boosted its application in various fields such as photo- and electrocatalysis,[3] gas-sensors,[4] energy storage and conversion,[5] and biomedicine.[6] To date, the main pitfall of BP remains its limited ambient stability,[7] as photoexcited electrons formed upon light exposure can be easily transferred to surface adsorbed O_2 molecules, giving rise to reactive O_2^- species which in turn easily break down the polyphosphorus layers resulting in the formation of P–O.[8] Therefore, since the initial rise of interest around BP, several studies have addressed the problem of its stabilization toward oxidation.[9] Effective passivation methods of BP via chemical routes include the coating with organic molecules,[7] the doping with metals as Te,[10] or the surface decoration with titanium complex,[11] silver cation[12] and transition metal nanoparticles like Au[13] and Ni.[14] Intriguingly, Ni infers a longer ambient stability to BP, paving the way to its wide utilization in the fabrication of long-lasting high performing devices.[15] Meanwhile the functionalization of 2D black phosphorus with Ni_2P NPs has been carried out[16,17] starting from a nickel (II) salt and abstracting P atoms of phosphorene as source of phosphorus, our group reported for the first time the functionalization of BP with Ni(0) NPs following two different strategies: a) immobilizing preformed Ni NPs capped with *n*-trioctylphosphine (TOP)[18] on 2D black phosphorene (Ni@TOP/BP) and b) growing Ni NPs *in situ* on BP nanosheets (Ni/BP).[15] It was demonstrated that gas sensors based on Ni/BP retained their electrical performance unaltered for one month,[15] while devices made with Ni@TOP/BP showed a drop in activity after only one week. Follow-up theoretical investigations[19] focusing on model system of Ni adatoms on few-layer black phosphorus have tried to explain the origin of this effect. It was predicted that the interaction between Ni and P atoms led to a downward shift of the conduction band that goes below the redox potential level of the O_2/O_2^- couple, which is included within the forbidden band gap in pristine BP, thus making the electron transfer of photo-excited electrons forbidden. However, no experimental investigations have ever been carried out to confirm this electronic modification, nor to address other mechanisms of ambient stabilization in Ni/BP. Herein, the band level diagram of BP, Ni@TOP/BP and Ni/BP (Figure 5) was derived using diffuse

[a] M. Vanni, M. Serrano-Ruiz, J. Filippi, M. C. Salvatici, M. Peruzzini, M. Caporali
Institute for the Chemistry of Organometallic Compounds (CNR-ICCOM)
Via Madonna del Piano 10
50019 Sesto Fiorentino (Italy)
E-mail: maria.caporali@iccom.cnr.it
[b] E. Fonda
Synchrotron SOLEIL
L'orme des Merisiers
91192 Gif-sur-Yvette (France)

Supporting information for this article is available on the WWW under https://doi.org/10.1002/cplu.202200457

Special Collection *Part of a Special Collection: "From Light to Heavy: Advancing the Chemistry of Pnictogen Compounds"*

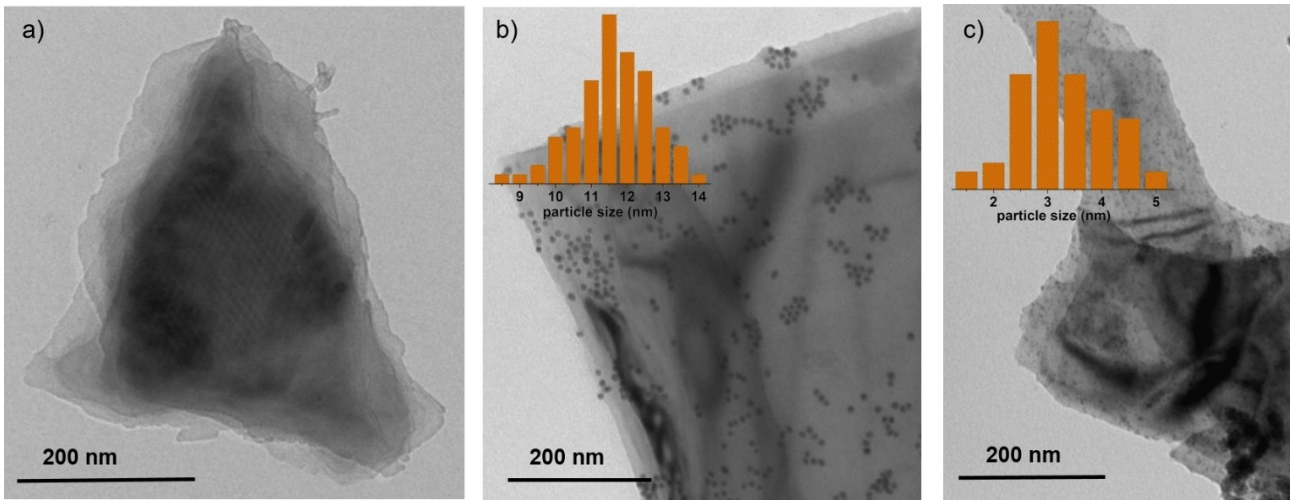

Figure 1. Bright field transmission electron microscopy (TEM) image of a) exfoliated BP, b) Ni@TOP/BP and c) Ni/BP with inset the size distribution of nickel nanoparticles.

reflectance UV-Vis spectroscopy and electronic impedance spectroscopy. Further structural insights on the intimate nature of the interaction between Ni and surface P atoms were gained from XAS spectroscopy, spreading light on the degradation mechanism and the reason of the different stability in ambient conditions observed for the three samples.

Results and Discussion

Bulk black phosphorus was exfoliated in DMSO under the action of ultrasounds (see ESI) and the resultant BP nanosheets were hybridized with nickel nanoparticles affording respectively Ni@-TOP/BP and Ni/BP heterostructures following two different procedures published previously.[18,15] The size and morphology of exfoliated BP and BP nanosheets functionalized with Ni NPs were checked by TEM.

As shown by Figure 1, the nanohybrids bear on their surface homogeneously dispersed NPs and meanwhile Ni@TOP/BP is characterized by preformed Ni NPs with spherical shape and average diameter $d = 11.5 \pm 0.9$ nm, Ni/BP has Ni NPs gown *in situ* and with a smaller diameter $d = 3.0 \pm 0.8$ nm. The different dimension is due to the capping agent TOP: when present, it imparts a precise dimension and morphology to the NPs, meanwhile when absent the growth of the nanocrystallites follows a different path responsible for the smaller average diameter. Further characterization by SEM-EDAX, XRD (see Figures S1–S5) and XPS (Figure S10) assessed the chemical identity and purity of the samples. UV-Vis diffuse reflectance spectroscopy (DRS) was conducted to evaluate the light absorption capability of the as-prepared materials and the corresponding absorbance spectra are shown in Figure 2.

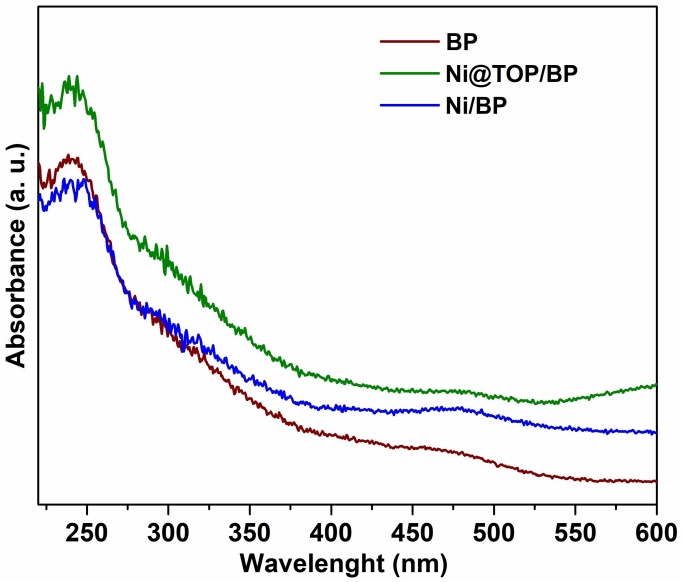

Figure 2. UV-Vis Absorbance spectra of BP, Ni@TOP/BP and Ni/BP.

Using the equation $[F(R)h\nu] = A(h\nu - E_g)^{n/2}$ where $n = 2$ being BP a direct band gap semiconductor, F is the diffuse reflection function, R is the data of the diffuse reflectance, A is an arbitrary coefficient, $h\nu$ is the incident photon energy, the value of the optical band gap E_g can be estimated.[20]

The corresponding Tauc plots are shown in Figure 3, where the extrapolation of the plot into the x-axis intercept gives an optical band gap of 1.15, 1.20 and 0.95 eV for pristine BP, Ni@TOP/BP and Ni/BP, respectively.

Electrochemical impedance spectroscopy is a powerful tool to probe the band structure of semiconductors and Mott-Schottky plots can provide the value of their flat-band potential (V_{fb}). The latter is ultimately related to the conduction-band edge of the semiconductor. As shown in Figure 4a–c, the flat-band potential is obtained from the extrapolation of the linear region of the plot to the *x*-axis. Correcting for the standard potential of the Ag/AgCl electrode (+0.2 V), the flat-band potential of pristine BP, Ni@TOP/BP and Ni/BP was calculated to be −0.23, −0.17 and 0.03 V *vs.* NHE (normal hydrogen electrode), respectively.

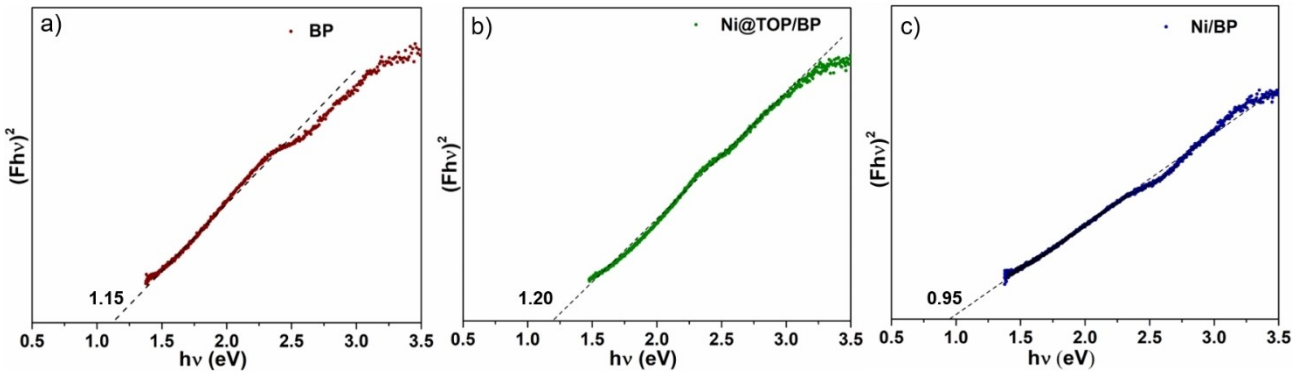

Figure 3. Tauc plots of (d) pristine BP, (e) Ni@TOP/BP and (f) Ni/BP are shown as function of photon energy hν (eV). Dashed lines show an approximate linear fit used to estimate the band gap.

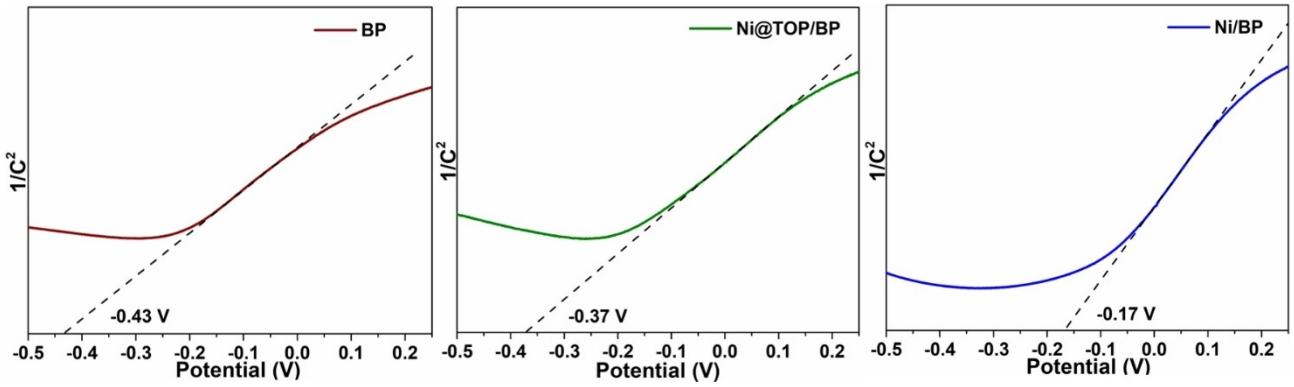

Figure 4. Mott-Schottky plots of (a) pristine BP, (b) Ni@TOP/BP and (c) Ni/BP. The values shown in the graphs are relative to Ag/AgCl reference electrode. Dashed lines show an approximate linear fit used to estimate the V_{fb}.

The flat-band potential can be approximate as *quasi Fermi level* of the semiconductor and lies 0.1 V lower the conduction band minimum (CBM).[21] Thus, the E_{CB} was estimated to be −0.33, −0.27 and −0.07 V for BP, Ni@TOP/BP and Ni/BP respectively. The energy position of the valence-band could then be calculated according to: $E_{VB}=E_{CB}+E_g$ where E_g is the band gap of the semiconductor and the band level diagram was derived and is reported in Figure 5. Remarkably, the relative position of VBM and CBM in pristine BP and Ni/BP follows the trend predicted by the theory,[19] with the two approaching each other and therefore the narrowing of band gap as an effect of the functionalization with Ni. In particular, a marked downward shift of 0.26 V in the position of the CBM is observed with Ni/BP compared to 2D BP. As this level is shifted below the redox potential of the O_2/O_2^- couple, this leads to the inhibition of electron transfer from the CB of Ni/BP to adsorbed O_2 following the formation of excitons by light adsorption. The lowering in CBM is also accompanied by a narrowing in band gap[22] of 0.20 eV, as predicted by previous DFT calculations.[19] On the other side, both the CBM position and the optical band gap observed in Ni@TOP/BP are very close to the values of pristine BP, the differences being only 0.06 V and 0.05 eV respectively, whose values are close to the experimental error.

This observation is reasonably accounted for by the distinct protocols used to introduce Ni NPs on the surface of BP flakes.

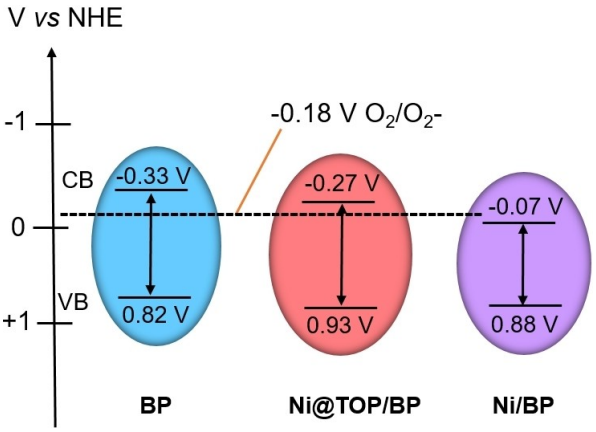

Figure 5. Energy band diagram of pristine BP, Ni@TOP/BP and Ni/BP. The redox potential of the couple O_2/O_2^- reported in the diagram as a dashed line, corresponds to an aqueous O_2 species and is a mere estimation of a surface adsorbed O_2.

While for Ni/BP the Ni NPs were grown *in situ* on BP, leading to the formation of a direct metal-phosphorus interface, with Ni@TOP/BP the Ni NPs capped with the ligand TOP were immobilized in a second step on the BP flakes. The presence of the ligand TOP at the surface of Ni NPs, as well as their introduction *ex situ*, likely prevent the building up of a strong

interaction with the BP surface and keep the electronic structure of the BP flakes almost unaltered in Ni@TOP/BP. This is also in perfect agreement with the previously observed minor ambient stability of BP in Ni@TOP/BP-based devices as compared to Ni/BP.[15] The different behavior of Ni@TOP/BP and Ni/BP towards oxidation was also highlighted by exposing the samples to ambient conditions (see Figure S9 for the temperature T (°C) and relative humidity RH% to which the samples were kept), and analyzing them by electron microscopy. In Figures S6-S8 the TEM images of the fresh samples are compared with the corresponding aged ones. It is evident how in Ni/BP the shape and dimension are kept intact during one month, while in Ni@TOP/BP the BP flakes appear swollen and the nanoparticles on the surface are not anymore detectable. In the case of pristine BP, the situation is even more dramatic, the flake edges are highly etched, demonstrating the pivotal role of nickel in improving the ambient stability as widely detailed in our previous work.[14]

Following the insight derived from the analysis of energy levels of BP, pointing to a distinct Ni–P interaction between Ni@TOP/BP and Ni/BP, and to deepen the understanding on the origin of the superior ambient stability of Ni/BP, a structural investigation was undertaken *via* X-Ray Absorption Spectroscopy (XAS) spectroscopy at the Ni *K*-edge, thus moving to the analysis of the metal chemical environment. Both fresh and aged samples, which were exposed to ambient conditions for different time (i.e. 0, 15 and 30 days), were analyzed. X-Ray Absorption Near Edge Structure (XANES) of reference materials such as bare Ni@TOP NPs, Ni_2P NPs, NiO and Ni foil (β-Ni) were measured for comparison, see Figure S11. Notably, the XANES spectrum of Ni@TOP/BP closely resembles the one of bare Ni@TOP NPs even after aging (see Figure 6), showing only a small increase in the peak at 8349 eV typical of NiO, arising from minor oxidation of the surface (see Figure S1). The XANES spectrum of fresh Ni/BP also resembles the profile of β-Ni and Ni@TOP/BP. However, the peak at 8349 eV which characterizes NiO (see Figure S11), is more pronounced upon aging, it points to a more severe oxidation of Ni in Ni/BP (see Figure 6).

This observation was accounted with the presence of the capping ligand TOP in Ni@TOP/BP, which acts as a protective shield around the surface, in agreement with previous inference, slowing down metal oxidation in this sample. Ni centers in Ni/BP instead, being naked, are exposed to the uptake of ambient oxygen, which suggest the existence of an additional mechanism of stabilization with Ni behaving as sacrificial reducing agent.

Important insights were gained on the nature of the interaction between Ni and P atoms in the nanohybrids. Though Ni_2P has been reported as being easily formed when using BP itself as a reducing agent in the presence of a nickel salt as source of Ni,[23] its presence in Ni/BP samples could be safely excluded for two reasons. Firstly, the observed distance between Ni centers in Ni/BP was 2.45 Å, resembling the Ni–Ni distance measured for β-Ni (2.48 Å), but shorter than the value of 2.56 Å, found for Ni_2P (see Table S1). Secondly, the XANES spectrum of Ni_2P showed a characteristic pre-edge feature at 8338 eV,[24] which is absent from both Ni/BP and Ni@TOP/BP. This is more easily appreciated from the second derivative plots shown in Figure 7.

Thus, the presence of nickel phosphide could be safely excluded from both samples and the nature of P–Ni interaction can be considered as a coordinative bond. The amount of Ni^0 has been estimated by a linear combination fit of the XANES spectra of two compounds: fresh Ni@TOP NPs and NiO, and it evolves from 100, to 92 and finally to 90% passing from fresh to 15 days and 1 month aged respectively, as reported in Table S1. Notably, all fits exclude Ni_2P for Ni@TOP/BP and Ni/BP, but Ni/BP spectra cannot be satisfactorily simulated by a simple linear combination and data are not shown.

Extended X-Ray Absorption Fine Structure (EXAFS) analysis (see Figure S12) provided an effective picture on the different oxidation behavior of the two samples. The Fourier transforms

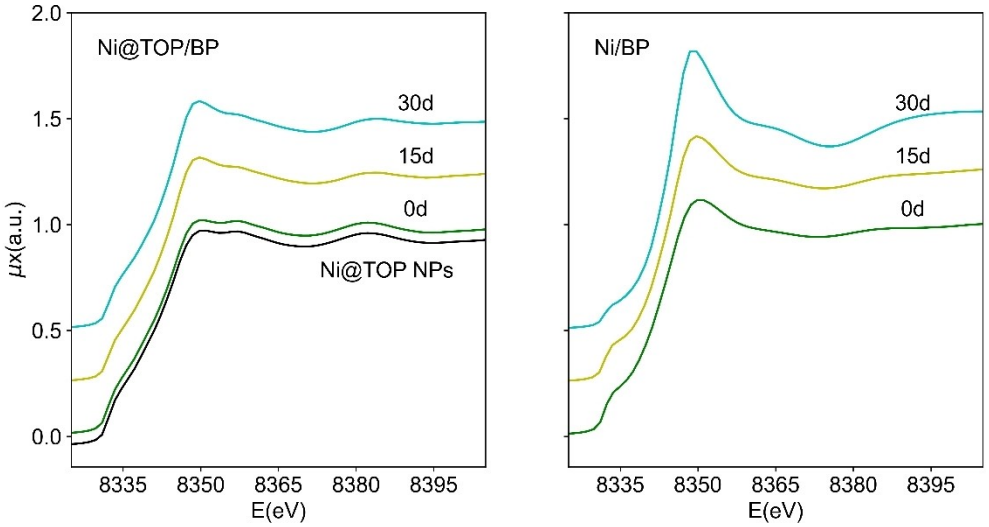

Figure 6. XANES spectra of Ni@TOP/BP and Ni/BP registered upon different time of exposure to ambient conditions (0, 15 and 30 days). In black, as a reference, the spectrum of a fresh sample of Ni@TOP NPs.

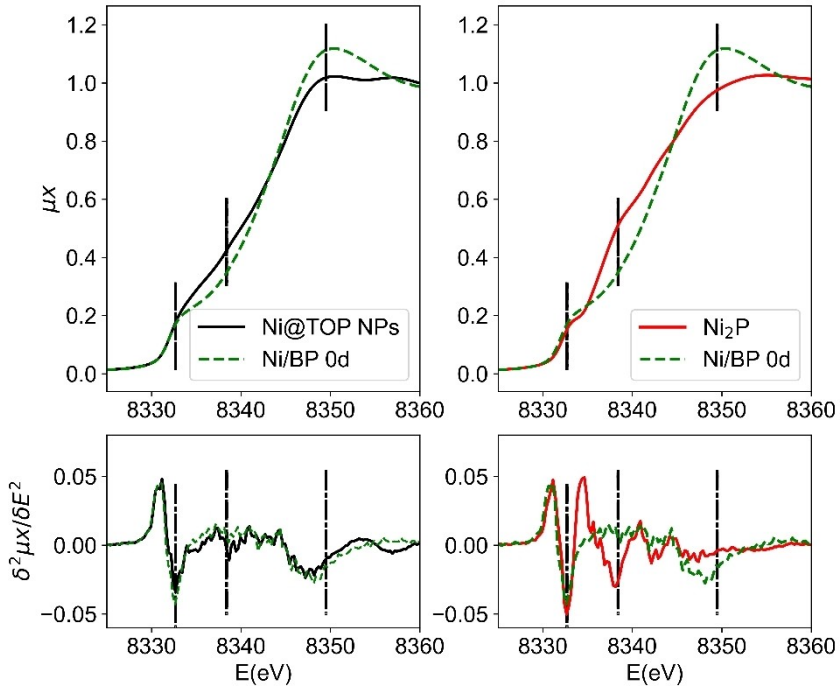

Figure 7. Comparing XANES and their second derivatives of Ni/BP with Ni@TOP/BP versus the reference Ni_2P.

of the k-weighed EXAFS spectra of Ni/BP and Ni@TOP/BP samples are shown in Figure 8.

From these spectra, a relevant distinction could be made between the two systems based on the interaction of Ni with the surface of BP. The FT spectrum of fresh Ni@TOP/BP featured a first coordination shell fitted with Ni–O bonds[25] at R = 1.94 Å and a second shell at R = 2.47 Å which corresponds to Ni–Ni distances (Table S3) being the experimental value of 2.48 Å in β-Ni[26] (Table S2), but there is no presence of Ni–P contributions. Remarkably, upon one-month air exposure, see Figure S9, the coordination number (CN) associated to Ni–Ni component diminished very slightly, from 7.2 to 6.1 (Table S3), and Ni–O vectors remained unaltered within the experimental error, in agreement with the partial nickel oxidation highlighted *via* XANES (see Figure 6).

Conversely, the fresh Ni/BP sample featured a first Ni–P coordination shell[27] at R = 2.27 Å, in addition to the Ni–Ni shell at R = 2.45 Å (Table S3). While the Ni–O contribution was absent

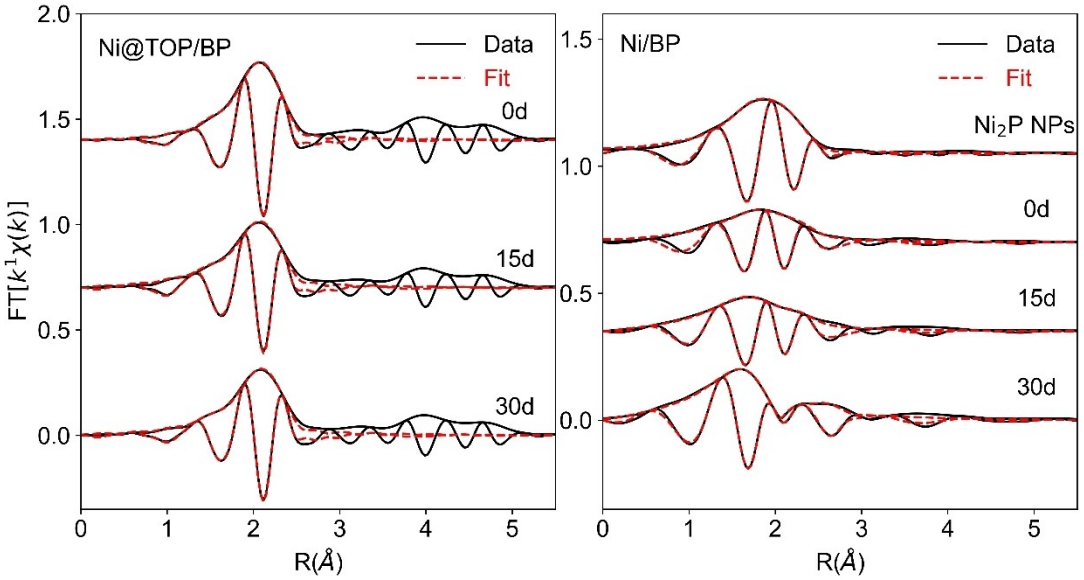

Figure 8. Magnitude of the Fourier Transforms of Ni@TOP/BP (left side) and Ni/BP (right side). As a reference, the FT of Ni_2P NPs has been added.

in fresh Ni/BP, this shell appeared upon 15 days of aging with R = 2.01 Å and CN = 1.9, increasing to CN = 2.6 after 30 days of aging. This is also consistent with the previous XANES observations, that point out the much higher nickel oxidation in Ni/BP in comparison to Ni@TOP/BP when exposed to ambient conditions, see Figure 6. Correspondingly, the Ni–Ni CN dropped from a value of 6 in fresh Ni/BP to 1.8 after 30 days of aging, due to the progressive formation of Ni–O bonds at the expense of Ni–Ni. The Ni–P bond distance of 2.27 Å pointed to a strong interaction between the surface of Ni NPs and BP (for comparison, the value measured in the Ni_2P standard was 2.24 Å), which corroborates the marked electronic modification of the BP energy levels previously described. Interestingly, the coordination of Ni to phosphorus was preserved with air exposure, as revealed by the Ni–P CN which remained almost unaltered, within the error bars (see Table S3 for precise values and errors bars). On the contrary, the average Ni–Ni coordination number in fresh Ni/BP rapidly decreased from CN = 6 to CN = 4 after two weeks of air exposure, and to CN = 2 after one month, highlighting a progressive fading of Ni–Ni bonds at the benefit of Ni–O, whose CN built up to approximately 3 over one month.

Finally, it must be noted the very short Ni–O distance found in Ni@TOP/BP series (1.94–1.96 Å) and the short one in Ni/BP (2.01 Å) versus NiO (about 2.08 Å),[25] can be related to the presence of Ni(3+), observed indeed by XPS, see Figure S10, which exhibits shorter distances than Ni(2+) and it is very close to Ni–O distance found for Ni(3+) substitution in perovskites.[28] Distribution of Ni–O distances may be broad and vary depending on the kind of oxide,[29] the shorter is 1.87 Å in Ni_2O_3 close to 1.89 Å in γ-Ni(OOH), but also to 1.90 Å as the first Ni–OH distance in α-$Ni(OH)_2$. Shorter and longer Ni–O distances coexist in these oxide and hydroxides, but they follow the general trend of shorter average distance for higher Ni oxidation state, confirming that there is a qualitative difference in the Ni oxide or hydroxide produced in the case of Ni@TOP/BP and Ni/BP samples. It is difficult to attribute the Ni–O distances to a definite structure, but this finding confirms that in average, Ni in Ni@TOP/BP and Ni/BP does not undergo the same type of oxidation.

Finally, combining the experimental data with previous DFT simulation performed on the nanohybrid Ni/BP,[19] the overall effect of Ni NPs functionalization on BP can be rationalized. Models to simulate the adsorption of O_2 molecule on the surface of pristine BP and Ni/BP were compared to spread light on the degradation mechanism. It was observed that by introducing nickel adatoms on the surface of BP, part of O_2 molecules from the surrounding atmosphere adsorb on Ni adatoms, decreasing the oxidation rate of the Ni/BP layer compared to bare phosphorene. In other words, Ni has the role of a sacrificial agent at local level, and undergoes the redox reaction where Ni adatoms in contact with O_2 give NiO, preserving BP from being attacked by O_2 molecules. A second operating mechanism, which is the electronic one, arises from the downward shift of the conduction band minimum under the level of O_2/O_2^- couple as predicted by calculations[19] and verified experimentally by us in this work, see Figure 5. The latter mechanism is not locally confined but propagates entirely the heterostructure; as a result, the electronic mechanism is the main responsible for the prolonged ambient stability and of course it is not influenced by the partial or not homogeneous coverage of BP flakes by Ni NPs.

Conclusions

For the first time, XAS spectroscopy was used as a real time analysis tool to follow the oxidation mechanism of BP flakes decorated with Ni NPs. Two different nanohybrids, Ni@TOP/BP and Ni/BP, were exposed to ambient conditions (0, 15 and 30 days) and were studied by XAS at the Ni *K*-edge to probe the coordination shell of the metal and its evolution once exposed to air. Intriguingly, a different change in both XANES and EXAFS profiles was observed when the two nanohybrids were exposed to ambient conditions. While in Ni@TOP/BP the oxidation of Ni was negligible thanks to the shielding effect exerted by the ligand TOP, in the case of Ni/BP the fraction of surface Ni atoms not involved in the coordination to phosphorus was easily attacked by O_2 molecules, thus potentially acting as sacrificial reducing agent. In addition, band level diagrams were derived for the two nanohybrids and for pristine BP by means of UV-Vis DRS and electrochemical impedance spectroscopy. A marked diminution in flat band potential and band gap was observed moving from pristine 2D BP and Ni@TOP/BP to Ni/BP, arising from the direct Ni–P interaction of the latter, providing the first experimental confirmation to previous calculations. This also led to identify the strong electronic effect resulting from the *in situ* functionalization with Ni as the additional and main mechanism responsible for the superior stability of Ni/BP.

Experimental Section

Chemicals

All the synthesis were performed under nitrogen atmosphere using standard air-free techniques. Anhydrous dimethylsulfoxide, trioctylphosphine (TOP) (97%), $Ni(acac)_2$ (95%), oleylamine (70%), red phosphorus (99.99%), tin and tin tetraiodide were used as received from Sigma Aldrich.

Liquid phase exfoliation of black phosphorus

Exfoliated black phosphorus (2D BP) was prepared by two steps-procedure. Firstly, bulk black P was synthetized from commercial high purity red phosphorus (99.99%) following a procedure reported in literature.[30] Afterwards, the obtained microcrystals of black P were exfoliated by ultrasonication in dimethylsulfoxide according to our previous work.[31]

Synthesis of Ni@TOP/BP and Ni/BP

The nanohybrids Ni@TOP/BP and Ni/BP were prepared as described in our previous work.[18,15]

Characterization

The morphology, shape and size of the flakes was analyzed via electron microscopy (TEM, SEM). A Shimadzu UV 2600 spectrophotometer was used for the measurement of UV-Vis diffuse reflectance spectroscopy. XRD characterization was conducted on a X'Pert PRO diffractometer with Cu Kα radiation. The chemical states of the samples were investigated via X-ray photoelectron spectrometry.

Electrochemical measurements

To obtain absolute band-edge positions with respect to water redox potentials, we fabricated the working electrode by coating the fluorinated tin oxide glass with the as-synthesized nanohybrids and we measured their flat band potentials, V_{fb}. The measurements were carried out by a standard three electrode cell on an electrochemical workstation (PARSTAT 2273 potentiostat), using a saturated Ag|AgCl|KCl electrode as the reference electrode, a platinum wire as the counter electrode and 0.5 M Na_2SO_4 aqueous solution as the electrolyte. To prepare the working electrode, pristine BP and the as-synthesized Ni@TOP/BP and Ni/BP nanohybrids were first dispersed in EtOH (1.5 mg/mL) by sonication for 20 minutes. The resulting ink was deposited by drop-coating on a fluorine-doped tin oxide (FTO) conductive glass substrate (4.0 cm^2) and was dried under a stream of nitrogen and then under vacuum. The measurements were run at a frequency of 1.2 KHz within the potential region −0.5 to 0.5 V vs Ag/AgCl reference electrode.

XAS measurements

XAS spectroscopy has been performed at the SAMBA beamline of Synchrotron SOLEIL (Saclay, Paris, France). The beamline monochromator employs two Si 220 crystals and the harmonic rejection has been performed by tuning the incidence angle over the two Pd coated Si mirrors at 5.5 mrad. Ni Ka fluorescence has been measured with a 36 pixels HPGe detector from Mirion technologies and data were acquired via XIA DxMap DSP cards. Data were dead time corrected. Data analysis has been performed with IFeffit[32] and Feff8.4 packages[33] fitting the data in r-space on the basis of theoretical standards. The S_0^2 value was fixed to 0.8 after checking this value on metallic Ni and Ni_2P standards. Linear combination fits of XANES spectra have been performed with Fastosh Software[34] over the interval 8300–8380 eV.

Acknowledgements

Thanks are expressed to the European Research Council (ERC) for funding the project PHOSFUN "Phosphorene functionalization: a new platform for advanced multifunctional materials" (Grant Agreement No. 670173) through an ERC Advanced Grant to M. Peruzzini. M.C. and M. S. R. acknowledge the project "FERMAT – Fast ElectRon dynamics in novel hybrid organic-2D MATerials" funded by the MUR Progetti di Ricerca di Rilevante Interesse Nazionale (PRIN) Bando 2017 – grant 2017KFY7XF. The authors acknowledge SOLEIL for funding proposal n. 20190470. M.C. S. acknowledges the CNR microscopy facility "Ce.M.E. – Centro Microscopie Elettroniche Laura Bonzi" for providing the facilities for the Gaia 3 (Tescan s.r.o, Brno, Czech Republic) instrument acquired thanks to "Ente Cassa di Risparmio di Firenze" Grant Number n.2013.0878 and Regione Toscana POR FESR 2014–2020 for the project FELIX (Fotonica ed Elettronica Integrate per l'Industria), Grant Number 6455. Open Access funding provided by Consiglio Nazionale delle Ricerche within the CRUI-CARE Agreement.

Conflict of Interest

There are no conflicts of interest to declare.

Data Availability Statement

The data that support the findings of this study are available in the supplementary material of this article.

Keywords: black phosphorus · energy band levels · nanostructures · nickel · passivation mechanisms

[1] R. Gusmão, Z. Sofer, M. Pumera, *Angew. Chem. Int. Ed.* **2017**, *56*, 8052–8072; *Angew. Chem.* **2017**, *129*, 8164–8185.
[2] M. Vanni, M. Caporali, M. Serrano-Ruiz, M. Peruzzini, *Surfaces* **2020**, *3*, 132–164.
[3] T. Yin, L. Long, X. Tang, M. Qiu, W. Liang, R. Cao, Q. Zhang, D. Wang, H. Zhang, *Adv. Sci.* **2020**, *7*, 2001431.
[4] Aaryashree, P. V. Shinde, A. Kumar, D. J. Late, C. S. Rout, *J. Mater. Chem. C* **2021**, *9*, 3773–3794.
[5] P. Li, J. Lu, H. Cui, S. Ruana, Y.-J. Zeng, *Mater Adv* **2021**, *2*, 2483–2509.
[6] A. Pandey, A. N. Nikam, B. S. Padya, S. Kulkarni, G. Fernandes, A. B. Shreya, M. C. García, C. Caro, J. M. Páez-Muñoz, N. Dhas, M. L. García-Martín, T. Mehta, S. Mutalik, *Coord. Chem. Rev.* **2021**, *435*, 213826.
[7] H. Song, H. Wu, T. Ren, S. Yan, T. Chen, Y. Shi, *Nano Res.* **2021**, *14*, 4386–4397.
[8] Q. Zhou, Q. Chen, Y. Tong, J. Wang, *Angew. Chem. Int. Ed.* **2016**, *55*, 11437–11441; *Angew. Chem.* **2016**, *128*, 11609–11613.
[9] Q. Li, Q. Zhou, L. Shi, Q. Chen, J. Wang, *J. Mater. Chem. A* **2019**, *7*, 4291–4312.
[10] B. Yang, B. Wan, Q. Zhou, Y. Wang, W. Hu, W. Lv, Q. Chen, Z. Zeng, F. Wen, J. Xiang, S. Yuan, J. Wang, B. Zhang, W. Wang, J. Zhang, B. Xu, Z. Zhao, Y. Tian, Z. Liu, *Adv. Mater.* **2016**, *28*, 9408–9415.
[11] Y. Zhao, H. Wang, H. Huang, Q. Xiao, Y. Xu, Z. Guo, H. Xie, J. Shao, Z. Sun, W. Han, X.-F. Yu, P. Li, P. K. Chu, *Angew. Chem. Int. Ed.* **2016**, *55*, 5003–5007; *Angew. Chem.* **2016**, *128*, 5087–5091.
[12] Z. Guo, S. Chen, Z. Wang, Z. Yang, F. Liu, Y. Xu, J. Wang, Y. Yi, H. Zhang, L. Liao, P. K. Chu, X.-F. Yu, *Adv. Mater.* **2017**, *29*, 1703811.
[13] Q. Wu, M. Liang, S. Zhang, X. Liu, F. Wang, *Nanoscale* **2018**, *10*, 10428–10435.
[14] M. Caporali, M. Serrano-Ruiz, F. Telesio, S. Heun, A. Verdini, A. Cossaro, M. Dalmiglio, A. Goldoni, M. Peruzzini, *Nanotechnology* **2020**, *31*, 275708.
[15] M. Valt, M. Caporali, B. Fabbri, A. Gaiardo, S. Krik, E. Iacob, L. Vanzetti, C. Malagù, M. Banchelli, C. D'Andrea, M. Serrano-Ruiz, M. Vanni, M. Peruzzini, V. Guidi, *ACS Appl. Mater. Interfaces* **2021**, *13*, 44711–44722.
[16] Y. Lin, Y. Pan, J. Zhang, *Int. J. Hydrogen Energy* **2017**, *42*, 7951–7956.
[17] J. Plutnar, Z. Sofer, M. Pumer, *RSC Adv.* **2020**, *10*, 36452.
[18] M. Caporali, M. Serrano-Ruiz, F. Telesio, S. Heun, G. Nicotra, C. Spinella, M. Peruzzini, *Chem. Commun.* **2017**, *53*, 10946–10949.
[19] S. Krik, M. Valt, A. Gaiardo, B. Fabbri, E. Spagnoli, M. Caporali, C. Malagù, P. Bellutti, V. Guidi, *ACS Omega* **2022**, *7*, 9808–9817.
[20] B. Tian, B. Tian, B. Smith, M. C. Scott, Q. Lei, R. Hua, Y. Tian, Y. Liu, *Proc. Nat. Acad. Sci.* **2018**, *115*, 4345–4350.
[21] W. Gao, X. Bai, F. Fan, Y. Zhou, C. Li, Z. Zou et al., *Chem. Commun.* **2020**, *56*, 7777–7780.
[22] Note that the same batch of exfoliated black phosphorus was used for running the two different functionalization with nickel. Thus, the difference in optical band gap registered by UV-Vis DRS is not due to

different layer thickness but it arises from an electronic effect connected to the functionalization with nickel.
[23] Z.-Z. Luo, Y. Zhang, C. Zhang, H. Teng Tan, Z. Li, A. Abutaha, X.-L. Wu, Q. Xiong, K. A. Khor, K. Hippalgaonkar, J. Xu, H. H. Hng, Q. Yan, *Adv. Energy Mater.* **2017**, *7*, 1601285.
[24] S. Hye-Ryun, C. Kye-Sung Cho, L. Yong-Kul, *Mater. Sci. Eng. B* **2011**, *176*, 132–140.
[25] A. Leineweber, H. Jacobs, S. Hull, *Inorg. Chem.* **2001**, *40*, 5818–5822.
[26] R. W. G. Wyckoff, *Crystal Structures.* 2nd ed., Vol. 1, Interscience Publishers, New York, **1963**, pp. 7–83.
[27] E. Larsson, *Ark. Kemi* **1965**, *23*, 335–365.
[28] T. Montini, M. Bevilacqua, E. Fonda, M. F. Casula, S. Lee, C. Tavagnacco, R. J. Gorte, P. Fornasiero, *Chem. Mater.* **2009**, *21*, 1768–1774.
[29] A. N. Mansour, C. A. Melendres, M. Pankuch, R. A. Brizzolare, **1994**, X-ray absorption spectra and structure of some nickel oxides (hydroxides); Defense technical information center, naval surface warfare center silver spring md: https://apps.dtic.mil/sti/citations/ADA281109.
[30] M. Köpf, N. Eckstein, D. Pfister, C. Grotz, I. Krüger, M. Greiwe, T. Hansen, H. Kohlmann, T. Nilges, *J. Cryst. Growth* **2014**, *405*, 6–10.
[31] M. Serrano-Ruiz, M. Caporali, A. Ienco, V. Piazza, S. Heun, M. Peruzzini, *Adv. Mater. Interfaces* **2016**, *3*, 1500441.
[32] M. Newville, *J. Synchrotron Radiat.* **2001**, *8*, 322–324.
[33] A. L. Ankudinov, B. Ravel, J. J. Rehr, S. D. Conradson, *Phys. Rev. B* **1998**, *58*, 7565–7576.
[34] G. Landrot, FASTOSH: A Software to Process XAFS Data for Geochemical & Environmental Applications. Goldschmidt, Boston (USA), **2018**.

Manuscript received: December 21, 2022
Revised manuscript received: February 7, 2023